# EXPERIMENTAL AND THEORETICAL STUDY ON THE ENERGY ABSORPTION OF COMPOSITE SQUARE TUBES UNDER QUASI-STATIC COMPRESSIVE LOAD

**Ramadan Omar Saied**

Mechanical and Industrial Department
Faculty of Engineering, University of Tripoli
E-mail:saied972004@yahoo.com,

**الملخص**

يقدم هذا البحث دراسة عملية ونظرية للطاقة الممتصة للأنابيب المربعة والمصنوعة من المواد المركبة أثناء تحطمها بقوى ضغط مسلطة محوريا عليها. ولغرض إجراء التجارب العملية تم صنع ثمانية أنابيب أبعادها (1000 × 100×100 مليمتر) بحيث كانت ثلاثة منها مصنوعة من الألياف الزجاجية، التي تميل بزاوية $\pm 45^{o}$ حول محور القالب، وثلاثة مصنوعة من الألياف الزجاجية، التي تميل بزاوية $0^{o}/90^{o}$ حول محور القالب، واثنان مصنوعتان من ألياف الكفلر، التي تميل بزاوية $0^{o}/90^{o}$ حول محور القالب. ولقد صنعت هذه الأنابيب بطريقة رص طبقات الألياف يدويا على قالب خشبي له نفس أبعاد الأنبوب وذلك بعد نقع الألياف بمادة البوليستر السائلة للصق الألياف. وبعد تصنيع وتجهيز الأنابيب تم تقطيعها إلى عينات بواسطة آلة قطع كهربائية بحيث أعدت خمس عينات من كل نوع بأطوال مختلفة حسب السمك والنسبة بين الطول والعرض. ولقد أجريت اختبارات التحطيم على العينات وذلك بتسليط قوة الضغط محوريا على كل عينة بواسطة آلة ضغط نوع Instron 4507 إلى أن تتحطم كليا. تم تصوير مراحل التحطيم فتغرافيا لكل عينة وسجلت نتائج الاختبارات أليا بواسطة جهاز الحاسوب وتم إظهارها على هيئة مخططات بين القوة المسلطة والإزاحة. كما أجريت اختبارات إجهادات الشد على عينات أعدت من الأنابيب لتحديد الخواص الميكانيكية لها مثل إجهادات الخضوع ومعامل المرونة ومعامل بواسون وتم إجراء الدراسة النظرية لعملية تشكل الأنابيب باستخدام نظريات التحطم الميكانيكي حيث استنتجت معادلات حساب الأحمال والطاقة الممتصة، كما تم تحديد أنماط وأساليب تحطم الأنابيب عن طريق إجراء الفحص العيني للعينات. ومن خلال النتائج المتحصل عليها وجد أن مخططات الحمل المسلط والإزاحة متشابهة لكل العينات وأن الطاقة الممتصة بواسطة الأنابيب المصنوعة من الألياف الزجاجية أقل من الطاقة الممتصة بالأنابيب المصنوعة من ألياف الكفلر. كما حددت أساليب التحطم بنوعين هما أسلوب تحطم منتظم وأسلوب تحطم غير منتظم ووجد توافق مُرضي بين القيم النظرية والعملية للحمل المتوسط والطاقة الممتصة.

**ABSTRACT**

This paper presents an experimental and theoretical study on the energy absorption characteristic of thin–walled glass woven roving reinforced polyester (GRP $0^{o}$ /$90^{o}$ and $\pm 45^{o}$) square tubes and Kevlar woven roving reinforced polyester (KRP $0^{o}/90^{o}$) tubes under quasi- static axial crushing load. Eight square tubes with dimensions of (100 × 100 × 1000) mm were manufactured using hand lay-up method and specimens were cut and fabricated from these tubes according to L/W ratio. All the tubes were tested using the Instron 4507 Testing Machine with maximum load cell of 200 kN. Load-displacement curves were obtained during the tests of specimens. In addition a description of the deformation processes of the tubes was discussed. It was concluded that a considerable energy was dissipated during the crushing of the tubes. Regular,

mixed and irregular fracture modes were observed. Loads carrying capacity of GRP tubes were found to be similar to those of KRP tubes while the mean load carrying capacity and energy absorption were lower in the case of GRP tubes.

**KEYWORDS:** Composite; Fiber glass; Kevlar; Energy absorption; Load; Crush.

## INTRODUCTION

Energy absorption in field of automotive structures is very important when one considers the effect of human life and safety in general. The design and development of energy absorbing devices have received much attention for engineers. One of the developments is the use of fiber reinforced composite materials as alternative to the traditional materials in the design of energy absorbing structures [1-3]. The fiber reinforced plastic composite has become an important class of materials because of its unique properties which include high specific strength, specific Young's modulus, high corrosion resistance, light weight and easy manufacturing processes [4]. The growth in the use of fiber reinforced composite material in structural crashworthiness has created the need to analyze and understand the behavior of composite structures under crushing loads. Considerable amount of research has been undertaken in recent years [5-7].

Energy absorption capability of composite tubes depends on the mechanism of the collapse mode which is a function of several factors such as arrangement of fibers, properties of the fiber-matrix interface geometry of the structures and others related to the test methods such as crushing speed and type of loads. These parameters have been investigated by many researches, for example Russell et al [8] undertook axial compressive tests on composite tubes to study the effects of parameters such as compression rate, thickness and filling foam on the crushing behavior and energy absorption capability. Price and Hull [9] studied the crushing behavior of square composite tubes made from random fiber glass reinforced polyester resin under static load and they found that the tubes crushed in progressive manner and their crushing mode depended on the geometry of the section, thickness and length of the tubes. Specific energy is defined as the energy absorption of the structure divided by mass. It can be also expressed in terms of other factors related to the instability of the structure [1]. Recently Sivakumar et al [10] expressed the energy observed in terms of specific energy in their study and they found that the most important parameter was the specific energy absorption (SEA). This study investigated experimentally and theoretically the energy absorption of glass fiber reinforced polyester composite square tubes under quasi-static compressive load.

## THEORTICAL ANALYSIS

In order to deduce a theoretical analysis of crushed composite tubes, it was assumed that the material of the tube is rigid up to failure. The fracture bending moment depends on the characteristic behavior of the composite material. The ends of the tubes are free to deform. The fold mechanism of regular mode is similar to the fold mechanism which was described by Wierzbicki and Abramowicz [11] for a thin walled metal tube. Figure (1) shows a schematic view of a composite square tube subjected to the quasi static load. The load is assumed to be uniformly distributed around the sides of cross-section. When the load gradually increases, a critical condition is reached and the

walls of the tube buckle in multiple sine wave configuration leads to deformation of the cross section (Figure 1-b). If the compressive load is increased above a critical value, the tube becomes unstable and starts to crumple in loops until become flatten (Figure 1-c). Figures (1-d - 1-f) show cross-section area of the tube before deforming after buckling and at final failure flatten respectively. It can be seen that the original right angle in each corner of the section remains unchanged which indicates that no bending moment is assumed to act between sides of the tube along the corners. Therefore, each side of the tube is analogous to a rectangular plate with simply supported edges [12].

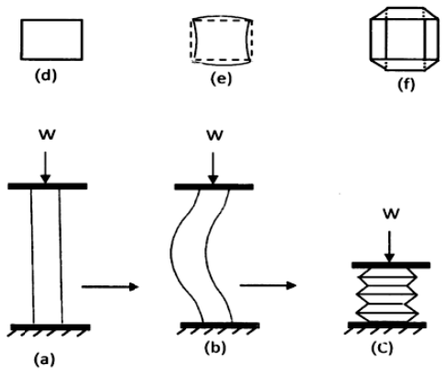


**Figure.1: A schematic view of a composite tube subjected to a quasi static load**

The mean load carrying capacity ($P_m$) of crushed composite tube can be determined by upper bound method using a kinematic admissible model (basic fold mechanism) described by Wierzbicki, and Abramowicz, [11] and the analysis given in detail by Reid and Reddy [13] as follows: consider a quadrant of the square tube of length (2H) (Figure 2-a) undergoing a compression (Figure 2-b) which gives the construction of basic fold mechanism [11].

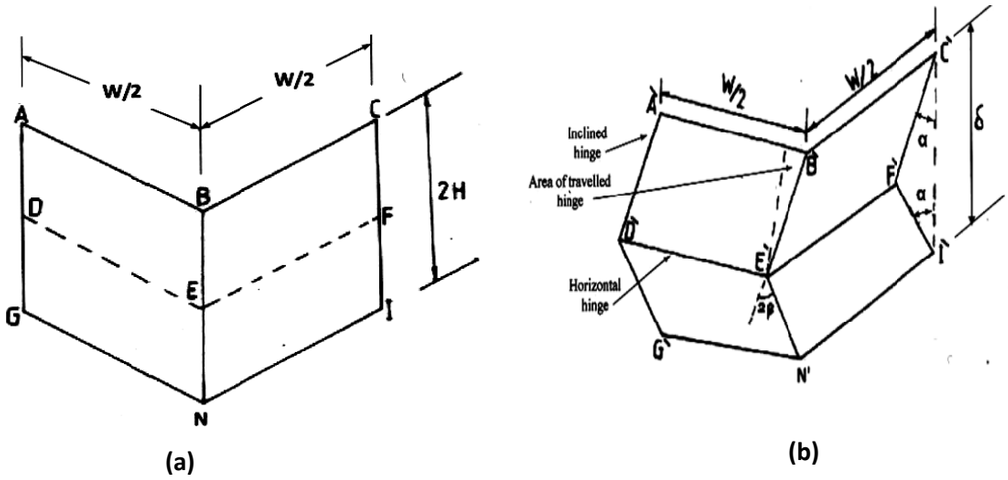


**Figure 2: A quadrant of the square tube of length (2H).**
**(a) Before deformation, (b) After deformation [13]**

The change in length of the tube can be described in terms of the instantaneous fold length (H) and the angle of bending (subtended angle (α) [13] as:

$$\delta = 2H\,(\,1 - \cos\alpha\,) \tag{1}$$

The central angle (β) at the section D' E'F' in Figure (2-b) by the following expression [13]:

$$\beta = \tan^{-1}(\sqrt{2\,\tan\alpha}) \tag{2}$$

Wierzbicki, and Abramowicz, [11] reported that for metal tubes there are three rate of energies dissipated must equal to the external work done in compression the basic fold mechanism as:

$$P\dot{\delta} = \dot{E}_1 + \dot{E}_2 + \dot{E}_3 \tag{3}$$

Where P is the compressive load and. $\dot{E}_1$ , $\dot{E}_2$ and $\dot{E}_3$ are the rate of absorbed energies by horizontal, inclined and travel hinges respectively. By adapting the analysis procedure of the energy absorption calculations given by Reid and Reddy [13] and using the above equation, the equilibrium load at any stage of compression for a composite square tube can be defined by (α) for complete tube section made up for quadrants is shown as:

$$P_\alpha = \frac{4}{\sin\alpha}\,[\,f_1\,M_1\,\frac{r}{t} + f_2 M_1\,\frac{W}{H} f_3 M_2\,\frac{H}{r}] \tag{4}$$

Where:

$$f_1 = 8\sqrt{2}\left(\,1 + \sin\frac{\beta}{2} - \cos\frac{\beta}{2}\right)\cos\alpha \tag{5}$$

$$f_2 = 2 \tag{6}$$

$$f_3 = 2\,\cos\alpha\,\sqrt{1 + sin^2\alpha} \tag{7}$$

Where ($M_1$) is the average fracture bending moment per unit width of fixed hinges of GRP $0^o/90^o$ tubes and assumed to be equal to fracture bending moment of a laminated plate of $0^o/90^o$. The value of ($M_2$) is the average fracture bending moment per unit width at inclined hinges and is assumed to be equal the value of fracture bending moment for laminated plate of ±45. (W) and (t) are the width and thickness of the element respectively. (H) and (r) are the instantaneous values of half fold length and radius of toroidal surface respectively. Reid and Reddy [13] stated that the values of (H) and (r) vary with the bending angle (α). However, Wierzbicki, and Abramowicz [11] showed that the mean value of (H) and (r) were found to be constant during the deformation process. The mean load carrying capacity ($P_m$) can be found by integration the equation (4) as:

$$P_m = \frac{4}{1 - cose\,\alpha}\,[M_1 k_1 \frac{r}{t} + M_1\,k_2\,\frac{W}{H} + M_2\,k_3\,\frac{H}{r}\,] \tag{8}$$

Where:

$$k_1 = \int_0^{\alpha_0} f_1 \, d\alpha \quad (9)$$

$$k_2 = \int_0^{\alpha_0} f_2 \, d\alpha \quad (10)$$

$$k_3 = \int_0^{\alpha_0} f_3 \, d\alpha \quad (11)$$

The mean value of (H) and (r) can be found by minimizing the $P_m$ with respect to (H) and (r) as follows:

$$\frac{\partial P_m}{\partial H_m} = 0 = -M_1 k_2 \frac{W}{H^2} + M_2 \, k_3 \frac{1}{r} \quad (12)$$

$$\frac{\partial P_m}{\partial r_m} = 0 = M_1 k_1 \frac{1}{t} - M_2 k_3 \quad (13)$$

Solving the equation (12 and 13), the values of (r) and (H) are:

$$r_m = \sqrt[3]{\frac{k_2 k_3}{k^2{}_1} \frac{M_2}{M_1} W t^2} \quad (14)$$

$$H_m = \sqrt[3]{\frac{k^2{}_2}{k_1 k_3} \frac{M_1}{M_2} W^2 t} \quad (15)$$

Taking$\alpha = \frac{\pi}{2}$, the values of $k_1 = 4.44$ , $k_2 = 3.14$ and $k_3 = 2.2956$ [13]. The mean values of (r), (H) and (P) can be found by substituting these values in equations (8), (14) and (15) as:

$$r_m = 0.715 \sqrt[3]{\frac{M_2}{M_1} W t^2} \quad (16)$$

$$H_m = 0.989 \sqrt[3]{\frac{M_1}{M_2} W^2 t} \quad (17)$$

$$P_m = 38 \sqrt[3]{M^2{}_1 M_2 (\frac{W}{t})} \quad (18)$$

The fracture bending moments per unit width (M1 and $M_2$) can be determined in terms of fracture stress per unit width [14] as:

$$M_1 = \frac{t^2}{4} \sigma_{f \mp 45} \quad (19)$$

$$M_2 = \frac{t^2}{4} \sigma_{f \mp 0/90} \quad (20)$$

By substitute equation (19) and (20) in equation (21) leads to:

$$P_m = 9.5 \sqrt[3]{t^2 W \left(\sigma_{f \mp 45}\right)^2 \left(\sigma_{f \mp 0/90}\right)} \quad (21)$$

Where:

W is the width of the tube
t is the thickness of the tube

$\sigma_{f\ \mp 45}$ is the fracture strength per unit width of the ±45° composite laminate
$\sigma_{f\ \mp 0/90}$ is the fracture strength per unit width of ±0/90° composite laminate

## MATERIALS AND EXPERIMENTS

### Materials

The specifications of the materials used to manufacture the composite square tubes and plates are shown in the Table (1).

**Table 1: Specifications of the fibers and resins**

| Material | Description |
|---|---|
| Glass fiber | E- 290 g $m^{-2}$ woven roving fiber cloth |
| Kevlar fiber | 190 g $m^{-2}$ woven roving fiber cloth |
| Resin | Scott-Bader, crystic 491 pa. pre–accelerated chemical resistant isphthalic polyester resin |
| Hardener | Catalyst, methyl ethyl ketone peroxide 50% in phlegmatizer. |

### Manufacturing and Preparing of Tube Specimens

Eight square tubes (100 mm ×100 mm ×1000 mm) were manufactured by hand lay-up method using a collapsible wooden mandrel. The hand lay-up method of a tube manufacturing was started by cleaning and covering the mandrel by a polyester film in order to get a smooth internal surface and easy removal of the tube from the mandrel. Woven roving clothes of glass 0°/90°, glass ± 45° and Kevlar 0°/90° were cut to layers according to the dimension (400 mm ×1000 mm for one lyre) and then wetted by a mixture of resin and catalyst, ratio (1:100). After that the wetted layers were carefully wrapped on the mandrel. The mandrel was placed between wood backing boards and whole assembly was clamped and left to cure at room temperature for approximately 12 hours. After curing, a tube was removed from the mandrel and then cut into desired specimens according to the ratio length to the width of the tube (L/W).

### Preparation of Tensile Test Specimens

In order to determine the material properties of the GRP and KRP tubes, several tensile test specimens were cut from composite plates having the same layers and materials as the tubes. All the specimens were prepared to their final dimensions (25 mm x 250 mm) according to the British Standard 2782, part 10: method 1003: 1977 [14]. The specimen's ends were reinforced with (25 mm x 50 mm) aluminum tabs using Araldite 2005 adhesive. All the specimens were strain gauged to measure the longitudinal and lateral strains.

### Experiments

The tests on the tubes were carried out using the Instron 4507 Test Machine with 100 kN and 200 kN load cells (Figure 3). The specimens were crushed by an axial load applied through flat parallel steel platens at a constant cross-head speed of 20 mm/min. The measured data of load and displacement were fed to the computer through the data logging system to obtain load-displacement curves. The tensile tests were carried out on

the specimens using the same machine with a 5 mm/min cross-head speed. Plots of stress versus strain can be obtained from the machine through the computer. Burn – Off test was implemented on samples to determine the volume fraction of the composite tubes according to the standard method [15].

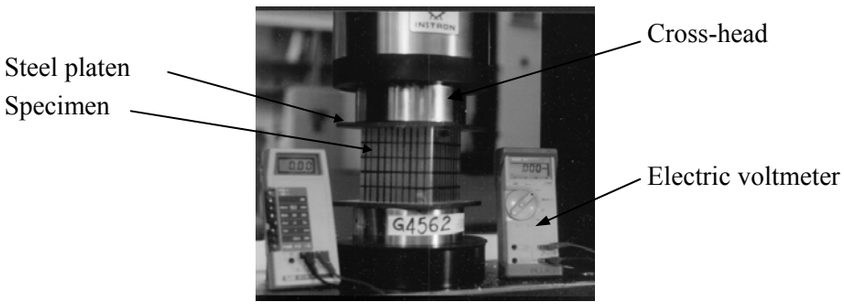


**Figure3: A photograph of the compressive test**

## RESULTS AND DISCUSSION

### Mechanical Properties

Table (2) shows the experimental results of the mechanical properties of the composite tubes. It can be seen that the failure strength and modulus are considerably affected by fiber orientation where the orientation $0^o$ /$90^o$ exhibited high values than the $\pm45^o$ and vise versa for fracture strains.

**Table 2: Mechanical Properties of composite tubes**

| Materials | $\sigma_f$ (MPa) | E (GPa) | $\varepsilon_f$ | $\nu_{12}$ | $v_f$ (%) | Mass of fiber (%) |
|---|---|---|---|---|---|---|
| GRP $0^o$ /$90^o$ | 299.5 | 17.7 | 0.02 | 0.165 | 40 | 56.6 |
| GRP $\pm45^o$ | 115 | 11.6 | 0.2 | 0.57 | 40 | 56.6 |
| KRP $0^o$ /$90^o$ | 332 | 19.5 | 0.02 | 0.11 | 40 | 44.5 |
| KRP $\pm45^o$ | 108.9 | 5.31 | 0.14 | 0.475 | 40 | 44.5 |

### Experimental and Theoretical Results of GRP and KPR Composite Tubes

Tables (3-a) - (3-h) show the experimental and theatrical results of maximum load carrying capacities ($P_{max}$), mean load carrying capacities ($P_m$), final compression percentage of the crushed tubes (C%), Energy absorption ($E_{total}$) and fracture modes of crushed tubes. It can be noted that there are small variations in the thickness in all the groups of layers due to the method of tube manufacturing (hand-layup method). The energy absorption was estimated by calculating the area under the curve of load-displacement curves and the fracture modes were identified by visual inspection of the crushed tubes after the tests. The compression percentage (C %) is the ratio of the final compression distance to the original length of the tube. The amount of energy absorption and the manner of fracture modes depend on the instability of the tubes under loads.

**Table 3-a: Results of two layers GRP $\pm45^o$ tubes**

| L/W | M (g) | t (mm) | C % | $P_{max}$ (exp) (N) | $P_m$ (exp) (N) | Pm (theo) (N) | $E_{total}$ (J) | Fracture Mode |
|---|---|---|---|---|---|---|---|---|
| 0.25 | 12 | 0.71 | 88 | 7920 | 2447 | 2447 | 46 | Regular |
| 0.5 | 26 | 0.8 | 92 | 6400 | 2650 | 2650 | 126 | Regular |
| 1 | 54 | 0.85 | 92 | 6350 | 2760 | 2760 | 294 | Irregular |
| 2 | 97 | 0.7 | 96 | 5000 | 2425 | 2425 | 379 | Irregular |
| 3 | 153 | 0.68 | 40 | 3540 | 2378 | 2378 | 180 | Irregular |

**Table 3-b: Results of four layer GRP ±45° tubes**

| L/W | M (g) | t (mm) | C % | $P_{max}$ (exp) (N) | $P_m$ (exp) (N) | $P_m$ (theo) (N) | $E_{total}$ (J) | Fracture mode |
|---|---|---|---|---|---|---|---|---|
| 0.25 | 28 | 1.36 | 86 | 31000 | 10770 | 5851 | 128 | Irregular |
| 0.5 | 40 | 1.12 | 94 | 14840 | 3680 | 5079 | 166 | Regular |
| 1 | 95 | 1.3 | 92 | 21000 | 5185 | 5260 | 471 | Regular |
| 2 | 188 | 1.44 | 95 | 21000 | 4270 | 5965 | 806 | Irregular |
| 3 | 299 | 1.57 | 61 | 12630 | 4430 | 6439 | 811 | Irregular |

**Table 3-c: Results of six layers GRP ±45° tubes**

| L/W | M (g) | t (mm) | C % | $P_{max}$ (exp) (N) | $P_m$ (exp) (N) | $P_m$ (theo) (N) | $E_{total}$ (J) | Fracture Mode |
|---|---|---|---|---|---|---|---|---|
| 0.25 | 30 | 1.9 | 80 | 62830 | 10050 | 12290 | 46 | Irregular |
| 0.5 | 63 | 1.8 | 88 | 38600 | 9320 | 11855 | 126 | Irregular |
| 1 | 133 | 2. | 92 | 41000 | 11930 | 12719 | 294 | Regular |
| 2 | 301 | 1.9 | 89 | 36000 | 12350 | 12290 | 379 | Regular |
| 3 | 447 | 2 | 95 | 33350 | 12000 | 12719 | 180 | Regular |

**Table3-d: Results of two layers GRP 0° /90° tubes**

| L/W | M (g) | t (mm) | C % | $P_{max}$ (exp) (N) | $P_m$ (exp) (N) | $P_m$ (theo) (N) | $E_{total}$ (J) | Fracture Mode |
|---|---|---|---|---|---|---|---|---|
| 0.25 | 13.8 | 0.82 | 86 | 5670 | 2110 | 4176 | 45 | Irregular |
| 0.5 | 21.28 | 0.5 | 95 | 4820 | 2410 | 3000 | 112 | Regular |
| 1 | 52 | 0.78 | 97 | 6780 | 1770 | 3835 | 165 | Irregular |
| 2 | 102 | 0.78 | 95 | 4500 | 3000 | 3835 | 386 | Regular |
| 3 | 145 | 0.6 | 92 | 4050 | 1580 | 3391 | 437 | Irregular |

**Table 3-e: Results of four layers GRP 0° /90° tubes**

| L/W | M (g) | t (mm) | C % | $P_{max}$ (exp) (N) | $P_m$ (exp) (N) | $P_m$ (theo) (N) | $E_{total}$ (J) | Fracture Mode |
|---|---|---|---|---|---|---|---|---|
| 0.25 | 24.5 | 1.5 | 82 | 21360 | 7350 | 4030 | 151 | Irregular |
| 0.5 | 46 | 1.7 | 94 | 18210 | 4860 | 4380 | 222 | Regular |
| 1 | 101 | 1.65 | 93 | 19270 | 4050 | 4294 | 374 | Regular |
| 2 | 207 | 1.69 | 94 | 19000 | 6520 | 4367 | 1224 | Irregular |
| 3 | 277 | 1.3 | 94 | 13840 | 3570 | 3663 | 473 | Regular |

**Table 3-f: Results of six layers GRP 0° /90° tubes**

| L/W | M (g) | t (mm) | C % | $P_{max}$ (exp) (N) | $P_m$ (exp) (N) | $P_m$ (theo) (N) | $E_{total}$ (J) | Fracture Mode |
|---|---|---|---|---|---|---|---|---|
| 0.25 | 32.5 | 2.06 | 80 | 95450 | 18200 | 7767 | 361 | Irregular |
| 0.5 | 55.32 | 2.2 | 83 | 55800 | 7300 | 8061 | 332 | Regular |
| 1 | 133.4 | 2.07 | 88 | 40900 | 10009 | 7742 | 959 | Irregular |
| 2 | 299 | 2.42 | 90 | 47100 | 10000 | 8593 | 1805 | Irregular |
| 3 | 422 | 2.26 | 93 | 40990 | 11170 | 8434 | 3109 | Irregular |

**Table 3-g: Results of two layers KRP 0° /90° tubes**

| L/W | M (g) | t (mm) | C% | $P_{max}$ (exp) (N) | $P_m$ (exp) (N) | $P_m$ (theo) (N) | $E_{total}$ (J) | Fracture Mode |
|---|---|---|---|---|---|---|---|---|
| 0.25 | 10.5 | 0.81 | 85 | 7390 | 2810 | 3836 | 58 | Irregular |
| 0.5 | 21.3 | 0.73 | 91 | 5920 | 1900 | 3600 | 85 | Irregular |
| 1 | 47.6 | 0.7 0 | 93 | 5660 | 3320 | 3409 | 308 | Regular |
| 2 | 79.9 | 0.72 | 97 | 4910 | 2640 | 3560 | 509 | Irregular |
| 3 | 115 | 0.72 | 80 | 3950 | 1650 | 3560 | 345 | Irregular |

**Table 3-h: Results of four layers KRP $0^o$ /$90^o$ tubes**

| L/W | M (g) | t (mm) | C% | $P_{max}$ (exp) (N) | $P_m$ (exp) (N) | $P_m$ (theo) (N) | $E_{total}$ (J) | Fracture mode |
|---|---|---|---|---|---|---|---|---|
| 0.25 | 24.7 | 1.89 | 82 | 46230 | 10850 | 8590 | 221 | Irregular |
| 0.5 | 38.7 | 1.5 | 94 | 15440 | 9500 | 6246 | 276 | Regular |
| 1 | 98.4 | 1.9 | 90 | 24240 | 8650 | 7313 | 861 | Regular |
| 2 | 185 | 1.9 | 92 | 20720 | 9150 | 7313 | 1674 | Regular |
| 3 | 257 | 1.7 | 92 | 15920 | 9600 | 7001 | 1926 | Regular |

## Mean Load Carrying Capacity

Figures (4) and (5) show the theoretical and experimental results of mean load carrying capacity of GRP±45º, GRP $0^o$ /$90^o$ ±45º and Kevlar $0^o$/$90^o$ crushed tubes versus thickness respectively. The theoretical values were calculated using equation (21) for tubes, which exhibited the regular folding mode. This is because of difficulty in indentifying the irregular folding mode with fold mechanism on which the analysis [11] is based.

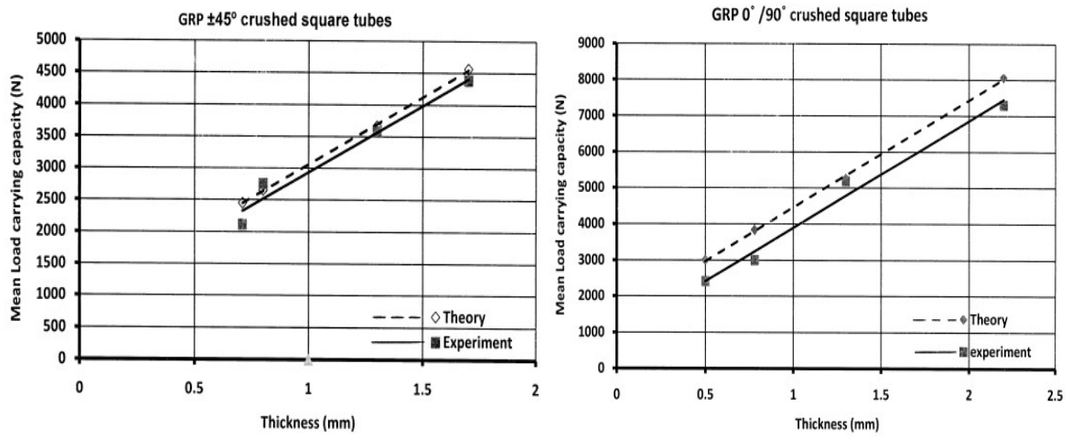


**Figure 4: Mean load carrying capacity versus thickness for GRP ±45ºand GRP 0˚ /90˚ tubes**

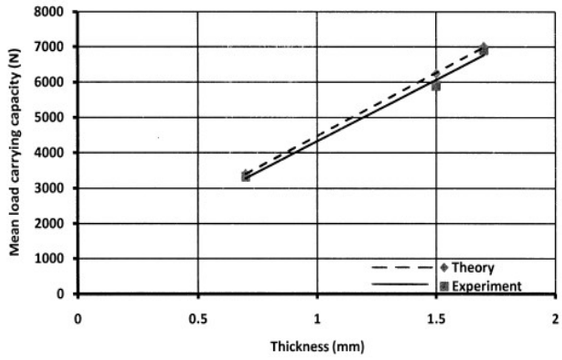


**Figure 5: Mean load carrying capacity versus thickness for KRP 0˚ /90˚ tubes**

It can be seen that the both mean loads increase with increase of tube thickness. The experimental values of mean load for GRP 0o /90o tubes are less than the theoretical values and this is probably related to the instability of the tubes during the crushing process. On the other hand, the GRP ±45o and Kevlar 0o/90o tubes show relatively reasonable agreement between theoretical and experimental values. The

difference may be related to the same reason of the GRP 0o /90o tubes or to the rigidity of the composite materials.

**Load-Displacement Curves**

Figure (6) shows the load- displacement curves of the GRP ±45$^o$ tube with L/W of 0.25 and GRP 0$^o$/90$^o$ crushed tube with L/W of 3 respectively. It can be seen that the curves show a large initial peak load corresponding to the initial collapse followed by rapid decrease in load due to instability of the tube. After this stage, the load reduced gradually and the curves becomes nearly flat in the short tubes with L/W of 0.25. This behavior was exhibited by all the short tubes. As the ratio of L/W increases, the curves exhibit a series of fluctuations about the mean load as shown in Figure (6b). The fluctuations consist of peaks and troughs corresponding to the deformation and folding of the tube. Figure (7) shows a comparison between the load – displacement curves for four layers GRP 0$^o$ /90$^o$ square tubes with L/W = 0.25, 0.5, 1, 2, and 3. Clearly it can be observed that the curves have similar manner and the mean loads carrying capacity are approximately comparable. The main function of the load-displacement curve is to estimate the energy absorption by calculating the area under the curves and to record the crushing history of the tubes.

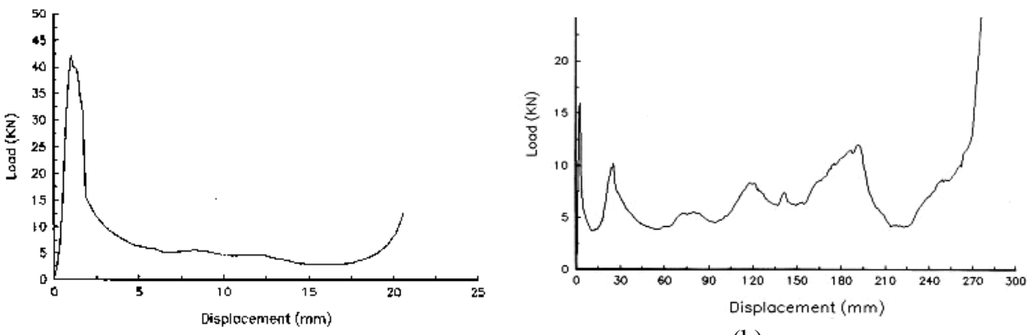


(a) (b)

**Figure 6: Load- displacement curves (a): GRP ±45$^o$ crushed tube with L/W of 0.25, (b): GRP 0$^o$/90$^o$ crushed tube with L/W of 3**

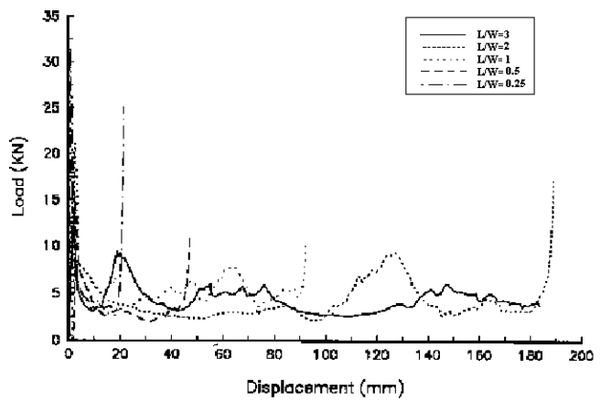


**Figure 7: Load-displacement curves for four layers GRP 0$^o$ /90$^o$ tubes**

**Fracture Modes**

Three types of fracture modes were observed experimentally during the crushing of the tubes. The first mode (Figure 8) is named as a regular fracture mode, in which the tube deformed with inextensional collapse mechanism [11]. In each fold of deformed tube, there are effectively four fixed horizontal and eight inclined hinges at the corner edges (Figure 9). The fixed horizontal hinges formed around the circumference at middle length of the tube, where two opposite sides folded inward, while the two other opposite sides folded outward. The inclined hinges form at AA´ and traverse the shaded area at BB´ at particular moment. Figure (10) shows the theoretical and experimental regular fracture modes for 6 layer GRP ± 45$^o$ tube with L/W of 2. The experimental fracture mode exhibited the same crushing process mentioned above. However, the fracture at the hinges occurred due to the effect of the thickness of the tube which allowed to the tube to exhibit more rigidity at the hinges.

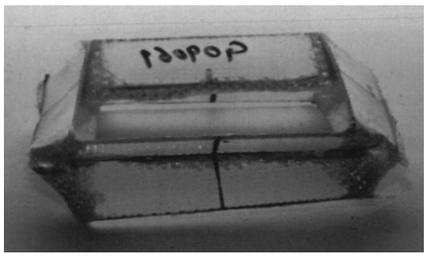

**Figure 8: The regular fracture mode of composite square tubes**

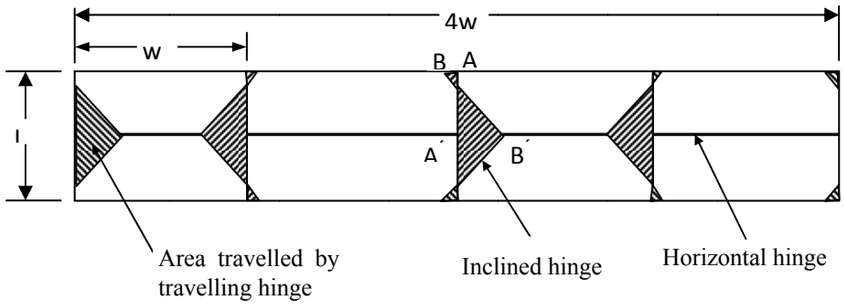


**Figure 9: Developed view of the tube deformed as above**

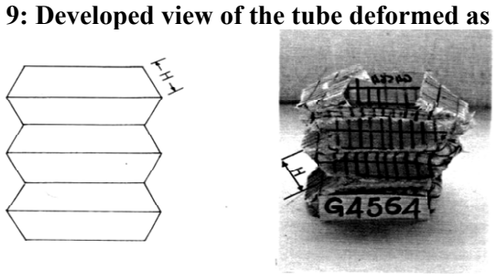

(a) (b)

**Figure10: Regular fracture mode for 6 layer of GRP ±45$^o$ tube with L/W of 2**
**(a) Theoretical mode, (b) Experimental mode**

Figure (11) shows the different stages of deformation process of a six layer Kevlar tube with L/W = 3. Photo (2) shows the collapse of the tube by buckling and formation

of the first fold or lobe at the bottom end. The other photos show continuation of the deformation in uniform manner. Photos 5 and 6 show fractures at the corners and at horizontal hinges more clearly

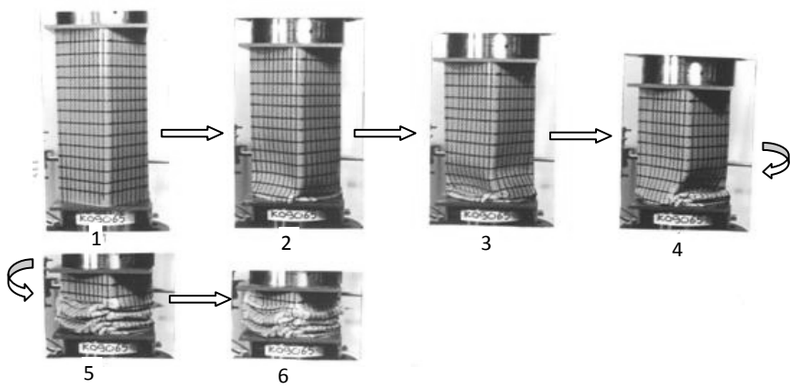


**Figure11 Deformation process of a six layer Kevlar tube with L/W = 3.**

Figure (12) show the fracture mode for two layer GRP $0^o/90^o$ tubes with L/W = 1 and 3 respectively. For the short tube, it can be seen that it deformed by inextensional collapse. However, because the material is rigid and brittle, fracture hinges appear and grow in a random manner through the sides of the tube (Figure 12-a). For tubes with ratio of L/W = 3, the tubes tended to buckle globally after the first lobe had formed and crumpling started due to the fracture hinges, which spread along the specimen in random manner (Figure 12- b).

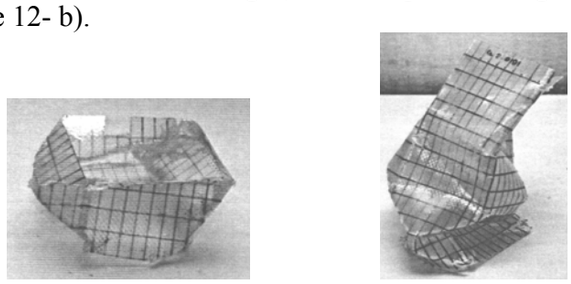

**(a) L/w =1** **(b) L/w =3**

**Figure: 12: Fracture modes for two layer GRP tubes,**

Figure (13) shows the crushing process of the GRP $0^o/90^o$ six layer tube with L/W = 4. It can be seen that the tube started to buckle with half sine wave on each faces (see photograph 2). As the load increased owing to the differences in rigidity and strength of corners and faces, the circumferential fractures started at the middle length of the tube with formation of a fold as shown in photograph (3) and (4). Photograph (5) shows the interpenetration failure of the tube. This type of failure has been observed by Thornton and Edwards [16] in some graphite and glass square tubes. Photograph (6) shows the completion of interpenetration failure mechanism, where the two halves of the tube enter into each other.

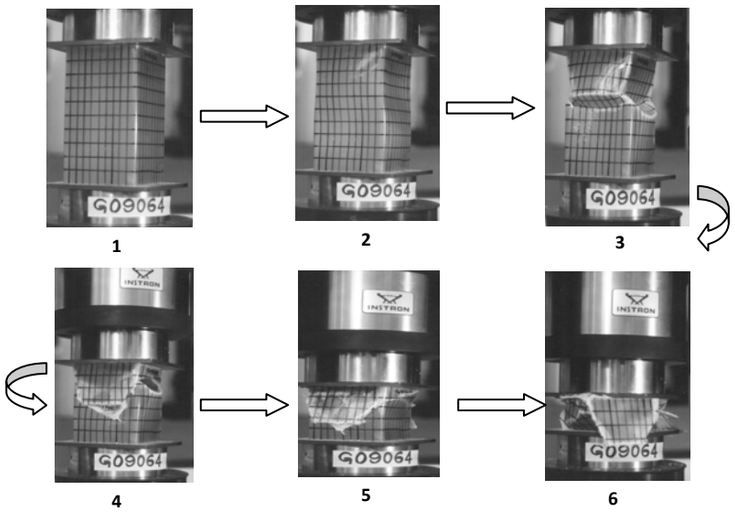


**Figure 13: Crushing process for GRP $0^o/90^o$ six layer tube with L/w =4**

## Effect of Wall Thickness on the Crushing Behavior

The increase in maximum load and energy absorption, have been observed in all cases with increase in tube thickness. The specific energy which is related to the increase in the stability of tube under loading, increases with increase in the wall thickness for all ratios examined as shown in Figure (14).

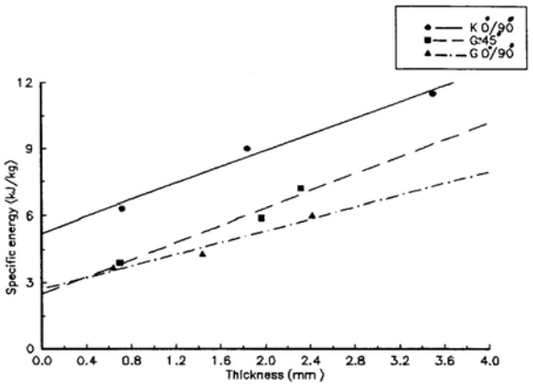


**Figure 14: Specific energy versus thickness for square tubes with L/W= 3**

The effect of the thickness on the fracture modes is absorbed in all cases except for W/L<1. The latter did not exhibit much variation in fracture modes, where some specimens exhibited regular deformation and others deform in random manner as shown in Figure (15)

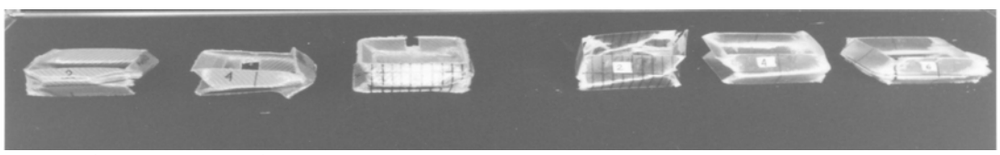


**Figure 15: Fracture modes for GRP and KRP crushing square tubes with L/W = 0.5**

Figure (16) shows the effect of the thickness on fracture modes for tubes with L/W =3. It can be seen that the two layer unloaded tube shows few fracture hinges and eliminations at the bottom, middle and top of the corners, whereas a four layer unloaded tube shows more but irregular and enhanced fractures and delamination at the bottom and the middle. Both unloaded suffer from sever buckling leads to tubes became unstable under applied loads. In the six layer tubes did not suffer from the instability and they completely fractured resulting in large fragments. It can be observed that the two and four layers unloaded tubes recovered a considerable energy due to the reduction of the wall thickness and nature of the matrix after unloading. This behavior of recovery has been observed in most cases of thinner tubes.

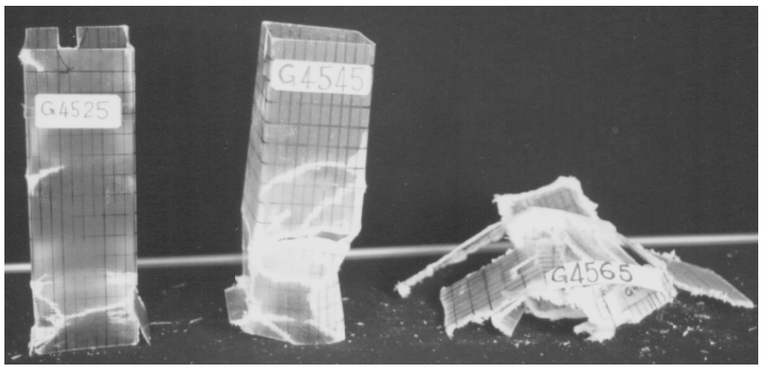


Two layer Four layer Six layer

**Figure 16: Unloaded GRP ±45o tubes after crushing**

Figure (17) shows the effect of the thickness on deformation process of KRP tubes during unloading after crushing. The thinning tube (two layers) deformed by buckling and crumpling whereas a four layer deform in regular manner and less instability. As the thickness increase from four layers to six layers, the tube became more stable, uniform and exhibited a greater degree of fracture at the corners and horizontal hinges.

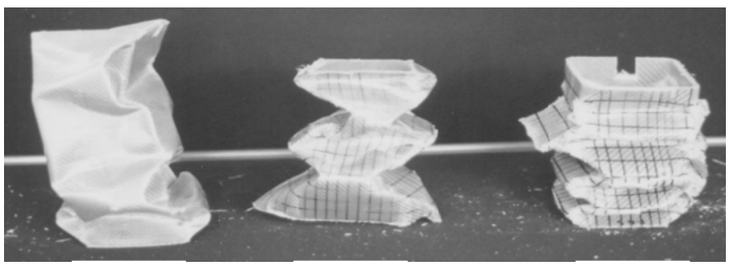

Two layer Four layer Six layer

**Figure 17: Unloaded KRP ±45$^{o}$ tubes after crushing**

## CONCLUSION

On the basis of the present investigation and discussion it can be concluded that two types of crushing modes (regular and irregular modes) have been observed during

the crushing of square tubes. Most of the KRP tubes with L/W > 1 tended to exhibit the regular mode whereas most the GRP tubes tended to exhibit the irregular modes. The values of maximum load, mean load carrying capacity and energy absorption of the GRP $0^o/90^o$ tubes were similar to that for GRP $\pm 45^o$ tubes and were lower than those for KRP $0^o/90^o$ tubes. The load displacement curves were similar and showed maximum peak load corresponding to the initial collapse followed by rapid decrease in load and a series of serrations and peaks about mean values. The thickness, type of fiber and fiber orientation had considerable effects on the mean load carrying capacity, crushing modes and energy absorption of the tubes.

**REFERNCES**


[1] Thornton, P. H., "Energy absorption in composite structures" Journal of Composite Materials Vol. 13, (1979).

[2] Farley, G.L., "Energy absorption of composite materials", Journal of Composite Materials", Vol. 17, (1983), 247-262

[3] Hamouda, b., Saied, O.R and Shuaeib, F. M., "Energy absorption capacities of square tubular structures", Journal of Achievements in Materials and Manufacturing Engineering, Vol. 24, No 1, (2007), 36-41

[4] Hull, D., "An Introduction to Composite Materials", Cambridge University Press, (1990).

[5] Thornton, P, H. and Jeryan, R.A., "Crush energy management in composite automotive structures", International Journal in Impact Engineering, Vol. 7, (1988), 167- 180.

[6] Yuqiu, Y., Asami, N, Hiroyuki, H and Kyoto, "Effect of Collapse Trigger Mechanism on the Energy absorption Capability of FRP Tubes",16th International Conference on Composite Materials, Japan (2007), 1-5

[7] Fadhil, A. and Mahdi, A., "The Effect of Composite Tubes Subjected to Axial Loading Comparing with the Number of Layers and Geometry", Australian Journal of Basic and Applied Sciences, Vol. 5, No 11, (2011), 607-616

[8] Russell, A.T., Reddy, T.Y., Reid, S.R. and Soden, P.D.,"Quasi-static and dynamic axial crushing of foam-field FRP tubes", Composite Materials Technology 1990(Eds D. Hui and Kosik) ASME, PD-7, (1991), 145-152.

[9] Price, J.N. and Hull, D., "Crush behavior of square section glass fiber polyester tubes", Fourth Annual Conference on Advanced Composites", (13-15 September 1988), Dearborn, Michigan, USA. 53-61.

[10] Sivakumar P, Wim, J. , Johan Van A. , Dimitrios K , Danny Van H , Jan W and John V, "Experimental study on the axial crushing behavior of pultruded composite tubes", Polymer Testing, Vol. 29, (2010), 224–23.

[11] Wierzbicki, T. and Abramowicz, W., "On the crushing mechanism of thin-walled structures", Journal Applied Mechanics, Vol. 50, (1983), 727-733.

12] Timoshenko, S.P. and Gere, J.M., "Theory of Elastic stability", McGraw-hill, New York, 1961.

[13] Reid, S.R. and Reddy, T.Y., "Axial Crushing of Foam-Filled Tapered Sheet Metal Tubes", Int. J.Sci., Vol. 28, No. 10, (1986), 643-656.

[14] Johnson, W. and Mellor, P.B, "Engineering Plasticity", Van Nostrand Reinhold Company, London, First edition (1973).

[14] BS 2782: Part 10: Method 1003, 1977.

[15] ASTM, D 3171-76 (Reapproved 1982),"Standard test method for fiber content of resin-matrix composite by matrix digestion.
[16] Thornton, P.H. and Edwards, P.J., "Energy absorption in Composite tubes", Journal of Composite Materials", Vol.16, (1982), 521-545.

**NOMENCLATURES**

| | |
|---|---|
| E | Young's Modulus |
| $\dot{E}_1$ , $\dot{E}_2$ and $\dot{E}_3$ | The rate of absorbed energies by horizontal, inclined and travel hinges respectively. |
| $f_{1,2,3}$ | Coefficients in equation (4) |
| $k_{1,2,3}$ | Coefficients in equation (8) |
| H, $H_m$ | Instantaneous and mean fold lengths |
| $M_{1,2,3}$ | Bending moments per unit width |
| L | Length of the tube |
| P, $P_m$ | Compressive load and mean load carrying capacity |
| $P_\alpha$ | Compressive load at a given compression defined by α |
| r, $r_m$ | Instantaneous and mean radii of troidal surface |
| t | Thickness of the tube |
| $\varepsilon_f$ | Fracture strain |
| $v_f$ | Volume fraction |
| W | Width of the square tube |
| α | Angle defining instantaneous compression of the tube |
| β | Angle defined the geometry of fold mechanism |
| δ | change in height of a fold unit |
| $\nu_{12}$ | Initial poission' s ratio |
| $\sigma_{f\ \mp 45}$ | Fracture stress of ±45$^o$ composite laminate |
| $\sigma_{f\ \mp 0/90}$ | Fracture stress of 0$^o$/90$^o$ composite laminate |
| GRP | Glass reinforced plastic |
| KRP | Kevlar reinforced plastic |